The exacerbation of soil acidification correlates with structural and functional evolution of the soil microbiome upon long-term agricultural intensification

Jie Shen
Sichuan Agricultural University https://orcid.org/0000-0002-4238-5055
Youlin Luo
Sichuan Agricultural University
Meng Li
Sichuan Agricultural University
Qi Tao
Sichuan Agricultural University
Philip J White
The James Hutton Institute
Edith Le Cadre
AGROCAMPUS OUEST
Yuting He
Sichuan Agricultural University
Bing Li
Sichuan Agricultural University
Qiquan Li
Sichuan Agricultural University
Qiang Xu
Sichuan Agricultural University
Yan Cai
Sichuan Agricultural University
Huanxiu Li
Sichuan Agricultural University
Yiding Li
Sichuan Agricultural University
Xiaoyan Tang
Sichuan Agricultural University
Lingke Guo
Sichuan Agricultural University

Junwen Zhao
Sichuan Agricultural University
Changquan Wang (w.changquan@163.com)
https://orcid.org/0000-0003-2038-4622

Research

Keywords: Agricultural intensification, Soil acidification, Metagenomics, Soil microbiome, pH homeostasis

Posted Date: January 22nd, 2020

DOI: https://doi.org/10.21203/rs.2.21635/v1

Abstract

Background: Agricultural intensification induces prolonged impacts on soil acidification (SA), whereas linking the mechanisms therein to structural and functional evolution of soil microbiota remain unclear, especially over longer time scales.

Methods: To investigate the short- and long-term effects of agricultural intensification on soil microbiome and its association with SA severity, we performed metagenomic sequencing of soil samples from typical rice-vegetable rotations for 0 (control, V0), 10 (V10), 20 (V20) years. The objectives were to clarify biomarkers that indicative of SA and its putative functions of acid production.

Results: Rice-vegetable rotations for 0, 10, 20 years yielded three well-defined soil clusters with differential acid saturation (V0: 4.5%; V10: 11.8%; V20: 40.7%). Soil pH declined significantly ($p < 0.05$) from the 6.38 (V0) to 4.82 (V20). Acid cations (H^+, Al^{3+}) dominating V20's exchangeable cation pool, suggesting that soils in V20 were highly acidic and acid-sensitive, which recruited distinct microbiomes. The increased acid cations and NO_3^--N concentrations are driving forces that lead to a higher abundance of Rhodanobacter , Gemmatirosa , Sphingomonas and Streptomyces in V20 samples, which acting as aciduric biomarkers that significantly and positively correlated with soil acidity. Furthermore, functional modules of microbial genes revealed V20 samples contained more genes associated with"oxidative phosphorylation" and "two-component system", particularly enriched multiple pathways of cytoplasmic pH homeostasis. More specifically, we found increased genetic abundances of active efflux of protons and cytoplasmic proton consumption in V20 samples over than in V0, which are both involved in the microbial dehydrogenation and acid production, and favoured the growth of Rhodanbacter , Gemmatirosa , Sphingomonas , Streptomyces .

Conclusions: Collectively, the identified aciduric biomarkers was closely associated with SA severity in intensive agroecosystems. An overall increase with the ongoing of intensive cropping history in the abundance of indicative genes associated with dehydrogenation and acid production pathways. The differential community compositions provide new clues to elucidate the interaction between the soil microbiome and SA severity, and varying dehydrogenation and acid production pathways provide novel insights into the exacerbation of SA.

Keywords: Agricultural intensification, Soil acidification, Metagenomics, Soil microbiome, pH homeostasis

Background

Agricultural land occupies ~40% of land surface and represents the largest land-use type on the planet [1, 2]. Currently, agricultural land across the worldwide urbanization have experienced or are experiencing conversions to high-input intensive agricultural purposes, including vegetables, orchard and grassland [3–6]. Simultaneously, half of globally fixed reactive nitrogen (Nr) fertilizes these agricultural areas, agricultural intensification thereby became the largest contributor to Nr pollution [7]. Soil acidification,

one of the major Nr pollution associated with agricultural intensification, can alter the biogeochemistry of soil ecosystems and adversely affect microbiota [8], and is a soil degradation process primarily due to active proton (hydrogen ion, H^+) overloads [9]. Indeed, the aciduric microbiotas thriving in highly acidic media have evolved with distinct mechanisms to the extreme stressors [10, 11], by which they can maintain a cytoplasmic pH of close to neutral in highly acidic media and therefore play pivotal roles in proton flows and acid production of the whole ecosystem [12, 13]. Whereas, the current insights into intensive agricultural practices only refers to the comparisons of same cultivation years, its prolonged impacts on soil microbiome and anthropogenic acidification has received less attention [14, 15]. Thus, it is of fundamental importance to determine the temporal changes in soil microbial communities of intensive agricultural systems, as well as their potential contributions to soil acid production.

Soil acidification is often accompanied by the changes in soil microbial composition, abundance and functions [16, 17]. Models for microbial distribution explains acidification development as result of the enrichment of aciduric microbiotas in response to long-term acidic stressors [18, 19]. In the past two decades, considerable attention examined the potential roles of aciduric microbiotas in acid production [13, 20, 21]. Approaches like microbial 16S rRNA gene sequencing and nitrogen-cycling network modeling have been applied for revealing the specific enrichment of aciduric microbiotas in acidic stressors, and have validated that microbial dehydrogenation mediated by these biomarkers was the key reaction of acid production process [22–25]. Recent studies on aciduric ammonia-oxidizing archaea (AOA) have promoted scientific interest and discussion on mechanisms of agricultural soil acidification. Among which, Candidatus Nitrosotalea and Nitrosopumilus have been confirmed as dominant microbiotas that are responsible for microbial dehydrogenation in the wider range of acidified cropland, grassland, and forest soils, leading to further H^+ loads and aluminum toxicity with the leaching losses of base cations [26–28]. In addition, variations in microbial communities largely originate from the inherent differences in microbial ability to cope with extreme environmental stressors [29]. Most archaea have functions maintaining their cytoplasmic pH within a narrower range than the pH outside the cell, termed “pH homeostasis”, while pH homeostasis in bacteria may be specific to particular species under acidic stressors, thereby bacteria tend to be more be more responsive than archaea to acidic stressors [30]. Previous studies have suggested that acidification independently caused by several different pathogenic bacteria, including Helicobacter pylori, Escherichia coli, Streptococcus mutans [31, 32], while in intensive agricultural systems, the information of exact aciduric biomarkers and its roles in acid production process remain largely unexplored. Consequently, soil microbial adaptation versus selection may result in a highly enrichment of aciduric biomarkers, which promotes microbial dehydrogenation and development of soil acidification, and therefore the soil with abundant aciduric biomarkers would be expected to have an increased risk of developing acidification compared to those within non-aciduric biomarkers.

More recently in metagenomic profiling, the availability of dominant soil microbial complete or near-complete genomes and their functions make it possible to disentangle the association of soil microbiome variations with changes in soil acidity, and to identify indicative functions responsible for these variations [17, 30]. Pioneer studies revealed the potential roles of pH homeostasis genes in microbial

dehydrogenation and acid production [32]. Prolonged periods of low pH stressors favour the growth of aciduric bacteria, leading to an increase of bacterial pH homeostasis genes [22, 33]. A major strategy for bacterial pH homeostasis is the use of transporters that catalyze active proton transport, including primary proton pumps like proton-pumping respiratory chain complexes and nicotinamide adenine dinucleotide phosphate (NADH) dehydrogenases, and secondary active transporters like cation-proton antiporters, which energize active proton uptake in exchange for cytoplasmic cations such as Na^+ or K^+ [32]. Another pH homeostasis strategy is related to metabolic consumption of cytoplasmic protons, particularly the catabolism of amino acids generates alkaline amines by decarboxylases, such as the lysine and arginine decarboxylases [34, 35]. Moreover, Tomb [31] and Chi A [36] et al. suggested proteomes of Acidithiobacillus ferrooxidans and Helicobacter pyloria could provide a passive adjunct to the active mechanisms for pH homeostasis, which formed a transient proton repellent to counteract external acidification. Overall, diverse mechanisms for pH homeostasis driven by functional genes impact microbial adaptation versus selection under acidic stressors. The multiple dehydrogenation pathways that mediating pH homeostasis are usually accompanied by the enrichment of environmental protons, thus the variation of acid production may be linked to diverse pH homeostasis gene-rich soil microbiomes.

Currently, urbanization has been increasing worldwide with rapid transition of populations from rural to urban, which means sharply increasing demands for grain and vegetables [37], and causing large amounts of conventional paddy fields have been converted from low nitrogen input “cereal cultivation” to high nitrogen input “vegetable cultivation” [38, 39]. These conversions have inevitably entailed extensive soil acidification and changes in microbial communities. Our previous studies have confirmed that intensive rotations would aggravate nitrogen enrichment and soil acidification [40, 41]. However, the prolonged effects of these intensive practices on soil microbial communities, as well as their contributions to soil acid production have not yet received enough attention.

We hypothesize that the exacerbation of soil acidification related to the decades-scale response of soil microbial community composition and its functional attributes following agricultural intensification in soils. Therefore, herein performed a metagenomic study of the soil microbiome in different intensive cropping history to thoroughly investigate the microbial components associated with the soil acidification. The objectives were to (i) clarify the temporal variation in soil microbial composition, abundance and functions upon agricultural intensification, especially its association with soil acidity, (ii) determine the aciduric biomarkers and indicative gene modules that are closely associated with acid production pathways, (iii) explain the interactions between the soil microbiome and the exacerbation of soil acidification.

Results

Altered soil acidity and high-order taxonomic composition upon short- versus long-term agricultural intensification

A highly soil acidification pH < 5 was found in long-term rice-vegetable rotations (V20) (Table 1). As shown in Fig. 1, soils in short- (V10) versus long-term rice-vegetable rotations were at acid-sensitive stage. Acid cations saturation ratios (proportion of H^+, Al^{3+}) were increased significantly with the ongoing of intensive cropping history ($p < 0.05$), which rose from 4.5% (V0) to 11.8% (V10) and 40.7% (V20). Concentrations of H^+ and Al^{3+} in V20 were 3.0 and 7.6 times higher than V0, respectively. Furthermore, soil base cations saturation ratios (proportion of Ca^{2+}, Mg^{2+}, K^+, Na^+) reached the amount to 95.5% in control treatment (V0), among which $Ca^{2+}$and Mg^{2+} dominated exchangeable soil cations pool and accounted for approximate 82.1% and 9.4%, respectively. By comparison, base cations saturation ratios significantly decreased to 88.2% in V10 and by 59.3% in V20.

To identify whether soil acidity can explain changes in microbial structure and functions among different intensive cropping history, we performed shotgun metagenomic sequencing on soil samples. A total of 549 million 150-bp paired-end reads were generated, with an average of 60.98 ± 2.73 (s.e.) million reads for each sample (Additional file 1: Table S1). After quality control, we obtained 543 million high-quality clean reads, with an average of 60.34 ± 2.69 (s.e.) million reads per sample (Additional file 1: Table S2). The clean reads were assembled, predicted and then aligned to the reference genomes from the National Center for Biotechnology Information (NCBI).

We found that soil microbial communities were disturbed after converting from conventional paddy (V0) to rice-vegetable rotations (V10 and V20) (Fig. 2a). Krona charts indicated that these changes in taxonomic composition were evident in high-order levels, particularly at class rank, which community structure shifted from a more balanced cluster comprising Betaproteobacteria, Deltaproteobacteria and Alphaproteobacteria in V0 to a less-balanced community comprising Alphaproteobacteria, Actinobacteria and Grammaproteobacteria dominated community in V10 and V20 (Fig. 2a, b). One-way ANOVA suggested, Betaproteobacteria, Deltaproteobacteria and Nitrospira were more abundant in V0 than in V10 and V20 ($p < 0.05$), whereas the relative abundances of Grammaproteobacteria, Gemmatimonadetes, Acidobacteriia, Ktedonobacteria and Sphingobacteriia were significantly increased in V20 than V0 ($p < 0.05$; Fig. 2c).

Shifts in fine-scale taxonomic composition and determine the aciduric biomarkers indicative of soil acidification

Furthermore, it is interesting to notice differentially fine-scale taxonomic compositions (Genus level) of soil microbiome in distinct intensive cropping history (Fig. 3 and Fig. 4a). V10 and V20 samples shared a similar microbial composition but showed a greater distance with V0 samples in both metagenome and 16S rRNA gene (Fig. 3a, c). Unconstrained principal coordinates analysis (PCoA) of Bray-Curtis distance revealed that microbial communities of V10 and V20 samples formed significantly distinct clusters with V0 in both metagenome (ANOSIM: statistic = 0.9835, $p < 0.05$) and 16S rRNA gene (ANOSIM: statistic = 1, $p < 0.05$), which separated along the first coordinate axis (Fig. 3b, d).

To characterize the core microbial composition and abundance, heat map analysis was performed with the top 50 most abundant genera (Fig. 4a). Increased abundance was evident at some dominant genera (e.g. Gemmatimonas, Bradyrhizobimu, Solirubrobacter, Gemmatirosa, Mycobacterium, Rhodanobacter, Arthrobacter and Preudolabrys, etc) of V10 and V20. The largest increase in relative abundance response to distinct intensive cropping history was by the genus Rhodanobacter, with the abundance increasing from an average of 0.06% [± 0.0086, s.e.] in V0 to 4.12% (± 0.6263, s.e.) of those in V20, followed by the genera Gemmatirosa, Gemmatimonas and Sphingomonas. The largest decrease was by the genus Nitrospira, with the abundance decreasing from an average of 1.65% [± 0.1325, s.e; V0] to 0.93 [± 0.0661, s.e; V20], followed by the genus Candidatus_Entotheonella and Geobacter.

Next, we analyzed whether these dominant members can be used as biomarkers to differentiate V0, V10 and V20. LDA scores (log 10) of 3.5 or greater are listed (Fig. 4b) to identify biomarkers for V0 and V20. The results showed that Nitrospira and Candidatus_Entotheonella were significantly enriched in V0, whereas Rhodanobacter, Gemmatirosa, Sphingomonas, Streptomyces, Haliangium, Candidatus_Solibacter and Thermogemmatispora showed higher relative abundance in V20 than V0. Furthermore, SparCC network analysis was constructed to investigate the possible interactions between the biomarkers. Two clusters were apparent from the network (Fig. 4c): Nitrospira, Candidatus_Entotheonella formed one cluster whereas Rhodanobacter, Gemmatirosa, Sphingomonas, Streptomyces, Haliangium, Candidatus_Solibacter and Thermogemmatispora formed the other. Intra-cluster associations were significantly (Spearman's rank correlation coefficient, $p < 0.05$) positive whereas inter-cluster associations were significantly negative.

Redundancy analysis (RDA) assessed the relationship between acidity parameters and dominant microbial communities and its implication for soil acidification. Acid cations (H^+, Al^{3+}) and inorganic nitrogen (NO_3^--N, NH_4^+-N) were positively (permutation test, $p < 0.05$) related with V20 samples, whereas base cations (Ca^{2+}, Mg^{2+}, Na^+) presented a notable positive correlation ($p < 0.05$) with V0 samples. Twelve genera with high correlation were listed in RDA (Fig. 4d). H^+, Al^{3+}, NO_3^--N and NH_4^+-N contributed positively ($p < 0.05$) to the distribution of Rhodanobacter, Gemmatirosa, Sphingomonas, Pseudolabrys, Gaiella, Candidatus_Solibacter, Streptomyces, while contributed negatively to Nitrospira, Candidatus_Entotheonella, Geobacter. Intriguingly, Rhodanobacter, Gemmatirosa, Sphingomonas, Candidatus_Solibacter, Streptomyces, Nitrospira and Candidatus_Entotheonella were above-mentioned biomarkers (Fig. 4b, c), thus they have potential for serving as acid-sensing biomarkers. Rhodanobacter, Gemmatirosa, Sphingomonas, Candidatus_Solibacter and Streptomyces acting as aciduric biomarkers.

Identifying differentially abundant KEGG modules in distinct intensive cropping history

To evaluated whether the shifts in soil microbial composition and abundance also had functional consequences concerning genes, we annotated the functions of genes that were specifically enriched in V0, V10 and V20 to Kyoto Encyclopedia of Genes and Genomes Orthology (KEGG) Module database. LEfSe analysis was performed and LDA scores (log 10) of 2 or greater are listed to identify indicative modules of V0, V10 and V20 respectively, which were related to 94 modules (Additional file 2: Table S3 ~

S5). Notably, most modules enriched in V0 samples were involved in ABC transporters, carbon metabolism, whereas modules enriched in V20 samples were related to oxidative phosphorylation, two-component system, DNA replication and nitrogen metabolism.

Second, using one-way ANOVA, we validated that modules were differentially enriched among sample groups (Tukey-Kramer test) (Fig. 5b). We found that gene clusters associated with functions supporting ABC transporters, e.g. branched-chain amino acid- (M00237), iron (III)- (M00190), tungstate- (M00186), phosphonate- (M00223), general L-amino acid- (M00232), manganese/zinc/iron- (M00319) transport system, were significantly enriched in V0 samples. Conversely, functional genes that were significantly more abundant in V20 samples were considerably related to multiple dehydrogenation pathways for pH homeostasis, which was typically represented by supporting proton-pumping: NAD biosynthesis (M00115), cytochrome complex oxidase (M00151, M00153, M00417), pentose phosphate pathway (M0004) and cytoplasmic proton consumption: GABA biosynthesis (M00135), assimilatory nitrate reduction (M00531).

Alteration in pH homeostasis gene modules likely drove differentially acid production of aciduric biomarkers

Finally, we want to figure out whether variation in soil acidity of sample groups were correlated with the 26 identified indicative modules. Results of spearman correlation analysis (Fig. 6a) showed that the concentrations of H^+, Al^{3+} and NO_3^--N were positively correlated with abundance of eleven modules significantly, including M0004, M00115, M00135, M00151, M00648, M00256, M00531, M00520, M00651, M00417 and M00523 ($p < 0.05$), while the base cations Ca^{2+}, Mg^{2+}, Na^+ were negatively correlated with these modules ($p < 0.05$).

To investigate the role of gene-annotated modules in the recruitment of soil microbiome, we carried out species and functional contribution analyses targeting the above-mentioned nine acid-sensing biomarkers (Fig. 4b) and eleven pH homeostasis modules (Fig. 6a). Regression analysis of Bray-Curtis distance in pH homeostasis modules and biomarkers community composition revealed that soil acid-sensing microbiomes of V20 samples were separated from V0 and V10 along the first two coordinate axes. Notably, these gene modules provided the largest contribution to Rhodanobacter (total abundance for eleven modules, Additional file 3: Table S6) and contributed (One-way ANOVA, $p < 0.01$) more to the V20 (425.56 ± 55.35) samples than the V10 (28.55 ± 4.62) and V0 (3.61 ± 0.50). The same variation and differences have been found in Gemmatirosa and Sphingomonas, which abundance rose from 24.88 ± 3.19 (V0) to 173.03 ± 17.46 (V20) and 37.20 ± 16.38 (V0) to 208.00 ± 24.54 (V20) respectively. Typically, as for Rhodanobacter, pH homeostasis modules, including M00004, M00531, M00135, M00115, M00151 and M00417 exhibited significantly higher abundance in V20 than V10 and V0 samples (Fig. 7a ~ f).

Discussion

Soil acidification is a major environmental issue of agricultural intensification, which is an acid production process driven by proton-generating reactions, such as microbial nitrification, dissociation of carbonic and other organic acids, accumulation of organic matter, and acid deposition, etc [9, 42]. When proton loads are elevated, base cations are exchanged out from soil sorption complex to buffer the input of acids [42]. As the leaching loss of base cations, soil pH becomes buffered by aluminum (Al^{3+}) mobilized from soils [9]. Although the practices of agricultural intensification have been proven to reduce the soil pH in our previous findings [41] as well as the general pattern of acidification observed in many other studies [13, 43], there has yet been no systematic study of the extent of soil acidification. Herein, we tested the impact of short- versus long-term rice-vegetable rotations on the composition pattern of cation pool in paddy soil. Figure 1 showed that soil exchangeable cation pool was dominated by acid cations (H^+, Al^{3+}) with pH dropped to 4.82 (Table 1) upon long-term rice-vegetable rotations. More importantly, we further found that long-term rice-vegetable rotations increased the magnitude of pH decline, where soils were at Al^{3+}-buffering stage with highly acidified and acid-sensitive. Overall, rice-vegetable rotations treatments, especially the V20 aggravated the soil acidification and acid-sensitivity. Under the gradient of acid saturation, soils in V0 could be characterized as base-enriched taxa (4.5%), and in V10 (11.8%) and V20 (40.7%) could be identified as acid-enriched taxa.

Given that these declines in soil pH may alter microbial biodiversity, and are intimately to soil functioning and in turn agroecosystems integrity [16, 17], we argue that changes of microbial biodiversity should be taken into account when assessing the impact of agricultural intensification on soil acidification. We revealed that base-enriched (V0) and acid-enriched (V10 and V20) soils recruited distinct microbiomes (Fig. 2, Fig. 3 and Fig. 4a). Gammaproteobacteria, Gemmatimonadetes and Acidobacteriia dominated the high-order taxonomic composition (class level) of V20 with dramatically declining in abundance of Betaproteobacteria and Deltaproteobacteria than V0, suggesting certain microbiota have the unique selectivity and thriving in acid-enriched soils. Microbiotas in intensive agricultural soils have been reported to be high sensitive to proton loads and subsequent soil acidification, and high acid saturation caused strong selective pressures on microbial community [44]. Selection minimizes microbial diversity and leads to the survival of dominant species, finally assembles the unique community structure, some of which shape biomarkers to adapt specific soil acidity [45, 46]. By LEfSe analysis (Fig. 4b) at fine-scale taxonomic composition (genus level), we found nine biomarkers: Nitrospira, Candidatus_Entotheonella, Rhodanobacter, Gemmatirosa, Sphingomonas, Streptomyces, Haliangium, Candidatus_Solibacter and Thermogemmatispora. Further SparCC network and RDA analysis (Fig. 4c, d) showed a strong influence of the acidity parameters on dominant microbial structure and distribution, which may explain the largest source of variation in soil microbiomes was differentially soil acidity along the intensive cropping history. In addition, we revealed potential aciduric characteristics of Rhodanobacter, Gemmatirosa, Sphingomonas, Candidatus_Solibacter, Streptomyces and potential alkaliphilic characteristics of Nitrospira, Candidatus_Entotheonella. Intriguingly, Rhodanobacter, Gemmatirosa, Sphingomonas, Candidatus_Solibacter, Streptomyces, Nitrospira and Candidatus_Entotheonella were above-mentioned biomarkers (Fig. 4b, c), thus they have potential for serving as acid-sensing biomarkers. Actually, previous studies have demonstrated the acid tolerance of Rhodanobacter [47], Sphingomonas [48],

Candidatus_Solibacter [49], Streptomyces [50]. A similar enrichment has been observed in acid-enriched soils of our study cohort as well, particularly for the dominant Rhodanobacter (Fig. 4a, b). One should note that Rhodanobacter belongs to the family Xanthomonadaceae, order Xanthomonadales and class Gammaproteobacteria of phylum Proteobacteria [51], and strains of which were isolated from a nuclear legacy waste site where co-contaminated with large amounts of acids, nitrate, metal radionuclides and other heavy metals, and have been found highly abundant and active in acidic, nitrate rich environments and high metal (e.g. uranium) concentrations [52]. Moreover, similar conclusion has been raised by highly abundant of Rhodanobacter in acidified agricultural soils, at pH near 4 [53], which is consistent with our findings that Rhodanobacter showed the survival potential in acid-enriched soils (pH 4.82). In our findings, the high correlation of acid cations and acid-sensing biomarkers further highlighted Rhodanobacter, Gemmatirosa, Sphingomonas, Candidatus_Solibacter and Streptomyces's essential role in serving as aciduric biomarkers, and call for further necessity in exploring whether aciduric biomarkers are the causal conducers to dehydrogenation and acid production.

Considering that environment and community structure drive the variations in ecosystem functions [54], any functional evolution that increases resistance represents an important strategy that may benefit stressful environment for microbiome. Concomitant with the alteration of soil acidity and microbial composition, we observed a functional evolution in microbiome. KEGG Module annotations with LEfSe analysis revealed that 94 KEGG modules were differentially enriched among the three groups (Additional file 2: Table S6), 15 and 19 modules that specifically enriched in V0 and V20 were listed in Fig. 5. Functional genes associated with ABC transporters, such as branched-chain amino acid, iron, tungstate and phosphonate, general L-amino acid, manganese/zinc/iron transport system were dramatically repressed in V20 samples. In contrast, oxidative stress, signal transduction and DNA repair genes were found actively enriched in V20, including oxidative phosphorylation, two-component system, DNA replication and nitrogen metabolism, etc. Moreover, spearman correlation analysis revealed the concentrations of H^+, Al^{3+} and NO_3^--N were positively correlated with abundance of 11 modules (Fig. 6a). Intriguingly, six out of eleven modules were above-mentioned (Fig. 5b) dehydrogenation pathways, including proton-pumping: NAD biosynthesis (M00115), cytochrome complex oxidase (M00151, M00417), pentose phosphate pathway (M0004) and cytoplasmic proton consumption: GABA biosynthesis (M00135), assimilatory nitrate reduction (M00531), suggesting that these modules might be involved in pH homeostasis of the soil microbiome in distinct acid saturated soils. Notably, these dehydrogenation pathways acting as a H^+ consumer and transporter, which have been reported to drive the difference in microbial pH homeostasis of distinct acidic media [30, 33]. The alteration in proton regulators suggested that aciduric microbiotas are likely to exhibit active dehydrogenation pathways for pH homeostasis and acid production in acid-enriched soils.

Ultimately, we provide evidence that pH homeostasis gene modules had the greatest contribution to Rhodanobacter in V20 than V0 samples (Fig. 6b, 7). Regression analysis in pH homeostasis modules and acid-sensing biomarkers community composition revealed that that pH homeostasis modules might have the role in establishment of the acid-sensing microbiomes (Fig. 6c). Previous studies showed that the

typical function of Rhodanobacter is their capability to undergo complete denitrification [53], which probably ascribed to the upregulation of nitrate reduction module in acid-enriched soils (Fig. 7d). Denitrification and associated denitrifying microorganisms are known to be strongly inhibited below pH 5, but Rhodanobacter thrives in conditions of low pH (pH 3–4), high nitrate (10–100 mmol) [47]. Indeed, it has been confirmed that dehydrogenation reactions triggered by pH homeostasis genes are the pivotal feature of acidophilic pathogens, such as Helicobacter pylori, Escherichia coli, Streptococcus mutans, and has been identified as an important contributor to acid production [31, 32]. Consequently, we described some supplementary clues of microbial acid tolerance, and hinted at a potential role of pH homeostasis gene modules in triggering microbial dehydrogenation and acid production reactions, while are likely responsible for recruiting a large proportion of aciduric biomarkers, especially Rhodanobacter.

Additionally, we found soils in V20 samples noticeably enriched genes associated with vancomycin resistance (M00651) and multidrug resistance (M00648) (Fig. 5b), illustrating the antibiotic resistance was abundant in V20 microbiome. It confirmed the concern that some of these resistance mechanisms may be exported from the “underground” world to the genomes of human pathogens [55]. Actually, alterations in pH homeostasis have been implicated in antibiotic resistance that low pH with upregulated proton pump could accelerate drug efflux [56, 57]. In our study, proton pumps modules as well as acid cations saturation in V20 shown highly coincided with those antibiotic resistance modules. We claim that better investigation of possible soil antibiotic resistance, particularly for inhibition of proton pumps, may be a clue used by aciduric microbiota to avoid drug efflux and acid accumulation in intensive agroecosystems.

Conclusions

Overall, this work represents the first step in the evaluation process of structural and functional evolution of the soil microbiome upon long-term soil acid exposure, and elucidate possible mechanisms underlying microbial role in maintaining pH homeostasis and aggravating acid production. Proving the concepts that long-term agricultural intensification: (a) increased soil acidity and acid-sensitive, and the exacerbation of soil acidification correlates with the enrichment of aciduric microbiotas; (b) yielded four well-defined aciduric biomarkers (Rhodanobacter, Gemmatirosa, Sphingomonas and Streptomyces) that contained more genes associated with cytoplasmic pH homeostasis and antibiotic resistance; (c) had diverse pathways for microbial pH homeostasis, especially dehydrogenation and acid production, as the proton transporter and consumer, are associated with the recruitment of a large proportion of aciduric biomarkers. The potential pH homeostasis pathways of aciduric biomarker are shown in Fig. 7. Simply put, (i) direct active efflux of protons by upregulated NAD biosynthesis, cytochrome complex oxidase and pentose phosphate pathway genes; (ii) cytoplasmic proton consumption by upregulated GABA biosynthesis and assimilatory nitrate reduction genes.

Methods

Study area and soil sampling

Study area is located at the national demonstration zone of “rice-vegetable production” in Tuojiang river basin of Chengdu Plain, Sichuan Province, China, which lies between 30°54' and 31°05 north latitude and 104°02' and 104°09' east longitude. It was chosen as a model site to represent the current expansive agricultural intensification occurring in Chengdu Plain and has been used extensively for long-term ecological monitoring by College of Resources, Sichuan Agricultural University. This area has a subtropical humid climate, a mean annual temperature of 15.9℃, precipitation of 867 mm and an altitude that ranges from 490 to 515 m above sea level. Soils are typical Percogenic Paddy Soils (Stagnic Anthrosols), and alluvial brown-grey material dominate the parent layer. The rapid urbanization of Chengdu megacity has led to the large adjustments of agricultural land-use in the past nearly two decades, particularly in the conversions of conventional paddy fields to rice-vegetable rotations [40]. According to the agricultural statistics of the Chengdu Statistical Yearbook (2000–2017), the area of cereal cultivation land decreased from 6.07×10^5 ha in 1990 to 3.45×10^5 ha in 2017, whereas rice-vegetable rotations land increased from 7.82×10^4 ha in 1990 to 1.84×10^5 ha in 2017.

The main sampling sites were from the same intensive farm (Qingjiang Community Farm), which were subdivided into three different intensive cropping history: (i) traditional rice-wheat rotations (non-conversion control treatment, V0); (ii) short-term (V10) versus (iii) long-term (V20) rice-vegetable rotations that were separately converted from rice-wheat rotations 10 and 20 years ago. In choosing sample plots, we aimed for consistency in soil texture (medium loam) and fertility (moderate). Each land-use is replicated (three plots per type) in a random block design, a total of 9 plots with 50 × 50 m (Table 1). Sampling was carried out on 16 April 2018, after growing season. At each plot, soil (0–20 cm) were sampled in 5 points, and the distance between each point was above 10 m [58]. Once sampled, all the samples from each site were manually pooled into one sample mixing [59], and were placed in aseptic-refrigeration boxes, then transported to the laboratory immediately. Each sample was divided into two parts, one was stored at 4 ℃ for physical and chemical analyses, whereas the other was stored at -80 °C until DNA extraction.

Physical And Chemical Analyses

Soil pH values (pH) was determined using a glass electrode by soil: water ratio = 1:2.5. Total nitrogen (TN) were measured with the Kjeldahi digestion procedure [60]. Organic matter (OM) was determined with dichromate oxidation [61]. Available phosphorus (AP) was determined with a spectrophotometer (UV2550, Shimadzu, Japan) [62]. Available potassium (AK) was measured by extraction with NH_4OAc on a flame photometer [63]. Ammonium nitrogen ($NH4^+$-N), nitrate nitrogen (NO_3^--N) were extracted with 2 mol L^{-1} KCl and determined using a Discrete Chemistry Analyzer (CleverChem380, Dechem-Tech, Germany). Exchangeable cations (H^+, Al^{3+}, Ca^{2+}, Mg^{2+}, K^+, Na^+) were extracted with 0.1 mol L^{-1} $BaCl_2$ (50: 1, solution: soil), then H^+ was determined using a glass electrode and Al^{3+}, Ca^{2+}, Mg^{2+}, K^+, Na^+ were measured with inductively coupled plasma mass spectrometry (ICP-MS, 7900, Agilent, USA) [42]. Each sampling site and the main characteristics along the conversion years are presented in Table 1.

DNA Extraction

Total DNA was extracted using FastDNA® SPIN Kit (MP Biomedicals, Southern California, USA) for Soil with 0.5 g of each sample and according to the manufacturer's instructions. The final DNA concentration and purification were determined by NanoDrop™ 2000 UV-vis spectrophotometer (Thermo Scientific, Wilmington, USA), and DNA quality was checked by 1% agarose gel electrophoresis. DNA was pooled into two aliquots and stored at -80 °C until for metagenome sequencing and16S rRNA sequencing.

Metagenome Sequencing And Gene Catalogue Construction

DNA was sheared into fragments of approximately 400 bp using an M220 Focused-ultrasonicator (Covaris Inc., Woburn, MA, USA). Afterwards, using NEXTFLEX™ Rapid DNA-Seq Kit (Bioo Scientific, Austin, TX, USA) to construct a paired-end library and following libraries were pooled and loaded by the way of Bridge PCR using NovaSeq Reagent Kits (Illumina, San Diego, USA). Above-mentioned metagenomic pair-end libraries were prepared and sequenced at Majorbio Bio-Pharm Technology Co. Ltd. (Shanghai, China) using NovaSeq 6000 platform (Illumina, San Diego, USA) (insert size 395 bp, read length 150 bp) and according to the standard protocol (http://www.illumina.com/).

Raw sequences were cleaned and assembled using Seqprep, Sickle (Version 1.33), Megahit (Version 1.1.2), and Newbler, and the length of contigs ≥ 100 bp were retained for further bioinformatics analyses [64]. MetaGene was used for ORF prediction (http://metagene.cb.k.u-tokyo.ac.jp/), and CD-HIT was used to cluster and build a non-redundant gene catalog (http://www.bioinformatics.org/cd-hit/). SOAPaligner (Version 2.21) was used for comparing high-quality reads with non-redundant gene catalog and obtaining statistical information of predicted gene abundance in corresponding samples (http://soap.genomics.org.cn/). Gene abundance was calculated by Transcripts Per Million reads (TPM): [(Reads Number/Gene Length)_Relative] × 100,0000 [65].

Metagenomic Annotation And Abundance Profiling

The taxonomic assignment (predicted genes clustered into metagenomic species) was carried out using BLASTP alignment against the integrated non-redundant (NR) database of the NCBI [66]. The abundance of a taxonomic specie was calculated by summing the abundance of genes annotated to a feature and the abundance of species in each sample was calculated at the taxonomic levels of domain, kingdom, phylum, class and genus, so as to construct the abundance table at the corresponding taxonomic level. High-order taxonomic composition for domain, kingdom, phylum and class level were visualized as Krona charts [67]. Fine-scale taxonomic composition for genus level were visualized as heat map with "vegan" package in R [68].

To assess the functional assignment, The NR gene catalog was aligned against the Kyoto Encyclopedia of Genes and Genomes (KEGG, http://www.genome.jp/kegg/) Module database [69] by BLAST (Version 2.2.28+, http://blast.ncbi.nlm.nih.gov/Blast.cgi) and assigned KEGG functional annotation by previously described methods with KOBAAS 2.0 [70]. The abundance of KEGG module was calculated by summing the abundance of genes annotated to the same feature.

16s Rrna Sequencing And Analysis

The V3-V4 hypervariable regions of the bacteria 16S rRNA gene were amplified with primers 338F (5'-ACTCCTACGGGAGGCAGCAG-3') and 806R (5'-GGACTACHVGGGTWTCTAAT-3') by thermocycler PCR system (GeneAmp 9700, ABI, USA) [71]. The PCR reactions were conducted using the following program: 3 min of denaturation at 95 °C, 27 cycles of 30 s at 95 °C, 30 s for annealing at 55 °C, and 45 s for elongation at 72 °C, and a final extension at 72 °C for 10 min. PCR reactions were performed in triplicate 20 μL mixture containing 4 μL of 5 × FastPfu Buffer, 2 μL of 2.5 mM dNTPs, 0.8 μL of each primer (5 μM), 0.4 μL of FastPfu Polymerase and 10 ng of template DNA. The resulted PCR products were extracted from a 2% agarose gel and further purified using the AxyPrep DNA Gel Extraction Kit (Axygen Biosciences, Union City, CA, USA) and quantified using QuantiFluor™-ST (Promega, USA) according to the manufacturer's protocol. Purified amplicons were pooled in equimolar and paired-end sequenced (2 × 300) on an Illumina MiSeq platform (Illumina, San Diego,USA) according to the standard protocols by Majorbio Bio-Pharm Technology Co. Ltd. (Shanghai, China).

Raw fastq files were quality-filtered by Trimmomatic and merged by FLASH with the following criteria: (i) The reads were truncated at any site receiving an average quality score < 20 over a 50 bp sliding window. (ii) Sequences whose overlap being longer than 10 bp were merged according to their overlap with mismatch no more than 2 bp. (iii)Sequences of each sample were separated according to barcodes (exactly matching) and Primers (allowing 2 nucleotide mismatching), and reads containing ambiguous bases were removed. Operational taxonomic units (OTUs) were clustered with 97% similarity cutoff using UPARSE(version 7.1 http://drive5.com/uparse/) with a novel'greedy'algorithm that performs chimera filtering and OTU clustering simultaneously. The taxonomy of each 16S rRNA gene sequence was analyzed by RDP Classifier algorithm (http://rdp.cme.msu.edu/) against the Silva (SSU128) 16S rRNA database using confidence threshold of 70% [72].

Statistical analysis

Differentially soil physicochemical properties, abundant species and KEGG modules were analyzed by ANOVA and ranked according to Tukey-kramer test ($p < 0.05$ or 0.01 or 0.001). The samples distances dendrogram and heat map were created with dissimilarity hierarchical clustering of metagenomic and bacterial16S rRNA genes based on beta diversity Bray-Curtis distance matrices that obtained from QIIME [73]; Principal Co-ordinates Analysis (PCoA) and Analysis of Similarity (ANOSIM) with Bray-Curtis distance tested whether sample groups are significantly different; a redundancy analysis (RDA) to test the relationships between acidity parameters, microbial community and samples, and permutest was employed to analyze the statistical significance of acidity parameters, and above-mentioned analysis were visualized in R "vegan" package [68].

Species And Functional Classifiers

To build potential classifiers like acid-sensing biomarkers and indicative KEGG modules for acidified identification, we performed linear discriminant analysis (LDA). Here, we applied on-parametric factorial Kruskal-Wallis sum-rank test with more strictly multi-group comparison strategy (all-against-all) to

identify taxonomic biomarkers and indicative KEGG modules that characterize statistical differences between soils with and without acidification; then wilcoxon rank sum test was used to investigate biological consistency of differences in subgroups, and LEfSe (the logarithmic LDA score threshold set at 2.0) was selected to estimate the effect of each component abundance on the differences (http://huttenhower.sph.harvard.edu/galaxy/root?tool_id=lefse_upload) [74]

Correlation And Contribution Analysis

Sparse correlations for compositional data (SparCC) network [75] was performed to construct the association network of above-mentioned biomarkers. Spearman's rank correlation was used to find correlations between acid-sensing biomarkers and identify potential aciduric biomarkers. Only significant correlations ($p < 0.05$) were linked in the network, and visualized in Python with "networkx" package.

Using correlation heat map analysis to identify indicative modules most likely correlate to acid cations: spearman's rank correlation was used to find correlations of acidity parameters and indicative modules, and visualized in R "pheatmap" package [76].

Statistical composition based on relative contribution (%) of indicative KEGG modules assigned to aciduric biomarkers were done using the method described by Ofek-Lalzar et al [77].

Abbreviations

SA:Soil acidification; NR:Non-redundant; KEGG:Kyoto Encyclopedia of Genes and Genomes; NCBI:National Center for Biotechnology Information; NRTs:Nitrate transporter; NAS:Assimilatory nitrate reductase; GadC:Glutamate/γ-aminobutyrate antiporter; GadB:γ-aminobutyric acid; GABA:γ-aminobutyric acid; G6PD:Glucose 6-phosphatedehydrogenase; NADP/NADPH:Nicotinamide adenine dinucleotide phosphate; Nuo:NADH-ubiquinone oxidoreductase; Cyt:Cytochrome complex; Q:Quinone pool; NAD/NADH:Nicotinamide adenine dinucleotide; AOA:ammonia oxidizing archaea; pH:Potential of hydrogen; TN:Total nitrogen; OM:Organic matter; AP:Available phosphorus; AK:Available potassium; NH_4^+-N:Ammonium nitrogen; NO_3^--N:Nitrate nitrogen; H^+:Hydrogen ion; Al^{3+}:Aluminum ion; Ca^{2+}:Calcium ion; Mg^{2+}:Magnesium ion; K^+:Potassium ion; Na^+:Sodium ion; ANOVA:Analysis of variance; ANOSIM:Analysis of similarities; LDA:Linear discriminant analysis; LEfSe:Linear discriminant analysis effect size; RDA:redundancy analysis; SparCC:Sparse correlations for compositional data; s.e.:Standard error.

Additional Files

Additional files 1: Statistics of metagenomic data sequence. Table S1. Characteristics of raw data sequence. Table S2. Characteristics of clean data sequence after quality control. (XLSX 11.9 kb)

Additional files 2: Indicative KEGG modules with LDA scores 2 in each sample groups. Table S3. KEGG modules that specifically enriched in V0. Table S4. KEGG modules that specifically enriched in V10. Table S5. KEGG modules that specifically enriched in V20. (XLSX 23.4 kb)

Additional files 3: Table S6. Contribution statistics of identified pH homeostasis gene modules on acid-sensing biomarkers. Bold font values are means (total functional contribution) of three replicate with standard error (s.e.). Different letters denote significant differences ($p < 0.05$) among conversion-years based on one-way ANOVA. V0 indicates conventional paddy fields (rice-wheat rotation, control), V10 and V20 indicate rice-vegetable rotations that were separately converted from conventional paddy 10 years and 20 years ago. (XLSX 23.9 kb)

Declarations

Ethics approval and consent to participate

Not applicable.

Consent for publication

Not applicable.

Availability of data and materials

Metagenomic sequencing raw data for all V10 and V20 samples have been deposited in NCBI Sequence Read Archive (SRA) database with BioProject accession number: PRJNA579552 and metagenomic sequencing raw data for all control (V0) samples have been deposited in NCBI Sequence Read Archive (SRA) database with BioProject accession number: PRJNA579335.

Competing interests

The authors declare that they have no competing interests.

Funding

This work was supported by National Key Research and Development Program of China (2017YFD0301701), National Key Research and Development Program of China (2018YFD0800605) and Research Programs of Sichuan Science and Technology Department (2018JY0002).

Authors' contributions

JS and CQW conceived and designed the overall study. JS, YLL, ML, LKG, JWZ and YDL coordinated the sample collection and analyzed soil physical and chemical properties. JS, YLL and ML carried out microbiome sample processing and performed the computational and metagenomic analysis. YTH and QX assisted with correlation and contribution analysis. QT, QQL, YC and HXL and interpreted the data

regarding metagenomics annotation. JS drafted the manuscript. YLL, ML and CQW contributed to the manuscript writing. QT, PJW, ELC and BL helped revise the final versions of the manuscript. All authors read and approved the final manuscript.

Author details

[1]College of Resources, Sichuan Agricultural University, Chengdu 611130, China. [2]The James Hutton Institute, Invergowrie, Dundee DD2 5DA, UK. [3]UMR Soil, Agro- and Hydro-systems, Spatialization (SAS), Agrocampus Ouest, Rennes, France. [4]Chengdu Popularization of Agricultural Technique Station, Chengdu 610041, China. [5]Fruit and Vegetable Research Institute, Sichuan Agricultural University, Chengdu 611130, China.

References

1. Foley JA, DeFries R, Asner GP, Barford C, Bonan G, Carpenter SR, et al. Global consequences of land use. Science. 2005;309(5734):570–574.
2. Tscharntke T, Klein AM, Kruess A, Dewenter LS, Thies C. Landscape perspectives on agricultural intensification and biodiversity – ecosystem service management. Ecol Lett. 2005;8:857–874.
3. Tian D, Niu S. A global analysis of soil acidification caused by nitrogen addition. Environ Res Lett. 2015;10(2):024019.
4. Tsiafouli MA, Thébault E, Sgardelis SP, de Ruiter PC, van der Putten WH, Birkhofer K, et al. Intensive agriculture reduces soil biodiversity across Europe. Global Change Biol. 2015;21(2):973–985.
5. Kong X B, Zhang F R, Wei Q, Xu Y, Hui J G. Influence of land use change on soil nutrients in an intensive agricultural region of North China. Soil Till Res. 2006;88:85–94.
6. Qi XX, Wang RY, Li JC, Zhang T, Liu LM, He YL. Ensuring food security with lower environmental costs under intensive agricultural land use patterns: A case study from China. J Environ Manage. 2018;213:329–340.
7. Bodirsky BL, Popp A, Lotzecampen H, Dietrich JP, Rolinski S, Weindl I, et al. Reactive nitrogen requirements to feed the world in 2050 and potential to mitigate nitrogen pollution. Nat Commun. 2014;5:3858.
8. Guo JH, Liu XJ, Zhang Y, Shen JL, Han WX, Zhang WF, et al. Vitousek PM, Zhang FS. Significant acidification in major Chinese croplands. Science. 2010;327(5968):1008–1010.
9. Boxman AW, Peters RCJH, Roelofs JGM. Long term changes in atmospheric N and S through fall deposition and effects on soil solution chemistry in a Scots pine forest in the Netherlands. Environ Pollut. 2008;156(3):0–
10. Baker-Austin C, Dopson M. Life in acid: pH homeostasis in acidophiles. Trends Microbiol. 2007;15(4):165–

11. Korzhenkov AA, Toshchakov SV, Bargiela R, Gibbard H, Ferrer M, Teplyuk AV, et al. Archaea dominate the microbial community in an ecosystem with low-to-moderate temperature and extreme acidity. Microbiome. 2019;7:11.
12. Barrie JD, Hallberg KB. Carbon, iron and sulfur metabolism in acidophilic micro-organisms. Adv Microb Physiol. 2008;54:201–
13. Chen LX, Huang LN, Méndez-García C, Kuang JL, Hua ZS, Liu J, et al. Microbial communities, processes and functions in acid mine drainage ecosystems. Curr Opin Biotechnol. 2016;38:150–
14. Steenwerth KL, Jackson LE, Calderón FJ, Stromberg MR, Scow KM. Soil microbial community composition and land use history in cultivated and grassland ecosystems of coastal California. Soil Biol Biochem. 2003;34(11):1599–1611.
15. Jangid K, Williams MA, Franzluebbers AJ, Sanderlin J, Reeves JH, Jenkins M, et al. Relative impacts of land-use, management intensity and fertilization upon soil microbial community structure in agricultural systems. Soil Biol Biochem. 2008;40(11):2843–2853.
16. Chen D, Wang Y, Lan ZC, Li JJ, Xing W, Hu SJ, et al. Biotic community shifts explain the contrasting responses of microbial and root respiration to experimental soil acidification. Soil Biol Biochem. 2015;90:139–
17. Tripathi BM, Stegen JC, Kim M, Dong K, Adams JM, Lee YK. Soil pH mediates the balance between stochastic and deterministic assembly of bacteria. ISME J. 2018;12:1072–
18. Kuang JL, Huang L, He Z, Chen LX, Hua Z S, Jia P, et al. Predicting taxonomic and functional structure of microbial communities in acid mine drainage. ISME J. 2016;10:1527–
19. Isobe K, Ikutani J, Fang Y, Yoh M, Mo JM, Suwa YC, et al. Highly abundant acidophilic ammonia-oxidizing archaea causes high rates of nitrification and nitrate leaching in nitrogen-saturated forest soils. Soil Biol Biochem. 2018;122:220–227.
20. Kuang JL, Huang LN, Chen LX, Hua ZS, Li SJ, Hu M, Li JT, Shu W S. Contemporary environmental variation determines microbial diversity patterns in acid mine drainage[J]. ISME J. 2013;7(5):1038–1050.
21. Chen LX, Hu M, Huang LN, Hua ZS, Kuang JL, Li SJ, et al. Comparative metagenomic and metatranscriptomic analyses of microbial communities in acid mine drainage. ISME J. 2014;9(7):1579–
22. Senneby A, Davies JR, Svensäter G, Neilands J. Acid tolerance properties of dental biofilms in vivo. BMC Microbiol. 2017;17(1):165.
23. Baker BJ, Banfield JF. Microbial communities in acid mine drainage. Fems Microbiol Ecol. 2003;44(2):139–
24. Isobe K, Ohte N. Ecological perspectives on microbes involved in N-cycling. Microbes Environ. 2014;29(1):4–
25. Kuypers MMM, Marchant HK, Kartal B. The microbial nitrogen-cycling network. Nat Rev Microbiol. 2018;16(5):263–276.

26. Könneke M, Bernhard AE, Torre JRDL, Walker CB, Waterbury JB, Stahl D A. Isolation of an autotrophic ammonia-oxidizing marine archaeon. Nature. 2005;437:543–546.
27. Herbold CW, Lehtovirta-Morley LE, Jung MY, Jehmlich N, Hausmann B, Han P, et al. Ammonia-oxidising archaea living at low pH: Insights from comparative genomics. Environ Microbiol. 2017;19(12):4939–4952.
28. Li Y, Chapman SJ, Nicol GW, Yao HY. Nitrification and nitrifiers in acidic soils. Soil Biol Biochem. 2018;116:290–
29. Young E, Carey M, Meharg AA, Meharg C. Microbiome and ecotypic adaption of Holcus lanatus (L.) to extremes of its soil pH range, investigated through transcriptome sequencing. Microbiome. 2018;6(1):48.
30. Slonczewski JL, Fujisawa M, Dopson M, Krulwich TA. Cytoplasmic pH measurement and homeostasis in Bacteria and Archaea. Adv Microb Physiol. 2009;55:1–79.
31. Tomb JF, White O, Kerlavage AR, Clayton RA, Sutton GG, Fleischmann RD, et al. The complete genome sequence of the gastric pathogen Helicobacter pylori. Nat. 1997;388:539–547.
32. Krulwich TA, Sachs G, Padan E. Molecular aspects of bacterial pH sensing and homeostasis. Nat Rev Microbiol. 2011;9(5):330–343.
33. Maurer LM, Yohannes E, Bondurant SS, Radmacher M, Slonczewski JL. pH regulates genes for flagellar motility, catabolism, and oxidative stress in *Escherichia coli* K-12. J Bacteriol. 2005;187(1):304–319.
34. Soksawatmaekhin W, Kuraishi A, Sakata K, Kashiwagi K, Igarashi K. Excretion and uptake of cadaverine by CadB and its physiological functions in *Escherichia coli*[J]. Mol Microbiol. 2004;51(5):1401–1412.
35. Gut H, Pennacchietti E, John RA, Bossa F, Capitani G, Biase DD, et al. *Escherichia coli* acid resistance: pH-sensing, activation by chloride and autoinhibition in GadB. EMBO J. 2006;25(11):2643–2651.
36. Chi A, Valenzuela L, Beard S, Mackey AJ, Shabanowitz J, Hunt DF, et al. Periplasmic proteins of the extremophile Acidithiobacillus ferrooxidans: a high throughput proteomics analysis. Mol Cell Proteomics. 2007;6(12):2239–2251.
37. Darilek JL, Huang B, Li DC, Wang ZG, Zhao YC, Sun WX, et al. Effect of land use conversion from rice paddies to vegetable fields on soil phosphorus fractions. Pedosphere. 2010;20(2):137–145.
38. Qin HL, Zhang JX, Zhu YJ, Lu J, Zhu YJ, Webster R, et al. Change from paddy rice to vegetable growing changes nitrogen-cycling microbial communities and their variation with depth in the soil. Eur J Soil Sci. 2016;67(5):650–658.
39. Wu L, Tang SR, He DD, Wu X, Shaaban M, Wang M, et al. Conversion from rice to vegetable production increases N_2O emission via increased soil organic matter mineralization. Sci Total Environ. 2017;583:190–201.
40. Luo YL, Li QQ, Shen J, Wang CQ, Li B, Yuan S, et al. Effects of agricultural land use change on organic carbon and its labile fractions in the soil profile in an urban agricultural area. Land Degrad

Dev. 2019;30:1875–1885.

41. Li QQ, Li AW, Yu XL, Dai TF, Peng YY, Yuan DG, et al. Soil acidification of the soil profile across Chengdu Plain of China from the 1980s to 2010s. Sci Total environ. 2019; doi:10.1016/j.scitotenv.2019.134320.
42. Mao QQ, Lu XK, Zhou KJ, Chen H, Zhu XM, Mori T, et al. Effects of long-term nitrogen and phosphorus additions on soil acidification in an N-rich tropical forest. Geoderma. 2017;285:57–63.
43. Li Y, Sun J, Tian D, Wang J, Ha D, Qu Y, et al. Soil acid cations induced reduction in soil respiration under nitrogen enrichment and soil acidification. Sci Total Environ. 2017;615:1535–1546.
44. Rousk J, Bååth E, Brookes PC, Lauber CL, Lozupone C, Caporaso JG, et al. Soil bacterial and fungal communities across a pH gradient in an arable soil. ISME J. 2010;4(10):1340–1351.
45. Gubryrangin C, Nicol GW, Prosser JI. Archaea rather than bacteria control nitrification in two agricultural acidic soils. Fems Microbiol Ecol. 2010;74(3):566–574.
46. Tripathi BM, Kim M, Singh D, Lee-Cruz L, Lai-Hoe A, Ainuddin AN, et al. Tropical soil bacterial communities in Malaysia: pH dominates in the equatorial tropics too. Microb Ecol. 2012;64:474–484.
47. Green SJ, Prakash O, Jasrotia P, Overholt WA, Cardenas E, Hubbard D, et al. Denitrifying bacteria from the genus *Rhodanobacter* dominate bacterial communities in the highly contaminated cubsurface of a nuclear legacy waste site. Appl Environ Microb. 2012;78(4):1039–1047.
48. Shi S, Bending GD. Changes to the structure of *Sphingomonas spp.* communities associated with biodegradation of the herbicide isoproturon in soil. Fems Microbiol Lett. 2007;269(1):110–116.
49. Rawat SR, Männistö MK, Bromberg Y, Häggblom M. Comparative genomic and physiological analysis provides insights into the role of Acidobacteria in organic carbon utilization in Arctic tundra soils. Fems Microbiol Ecol. 2012;82(2):341–355.
50. Bonde MR, Mcintyre GA . Isolation and biology of a Streptomyces sp. causing potato scab in soils below pH 5.0. Am J Potato Res. 1968;45(8):273–278.
51. Nalin R, Simonet P, Vogel TM, Simonet P. *Rhodanobacter* lindaniclasticus gen. nov. sp. nov. a lindane-degrading bacterium. Int J Syst Bacteriol. 1999;49(1):19–23.
52. Prakash O, Green SJ, Jasrotia P, Overholt WA, Canion A, Watson DB, et al. *Rhodanobacter denitrificans sp. nov.*, isolated from nitrate-rich zones of a contaminated aquifer. Int J Syst Evol Micr. 2012;62:2457–2462.
53. Heuvel RNVD, Biezen EVD, Jetten MSM, Hefting MM, Kartal B. Denitrification at pH 4 by a soil-derived Rhodanobacter-dominated community. Environ Microbiol. 2010;12(12):3264–
54. Orland C, Emilson EJS, Basiliko N, Mykytczuk NCS, Gunn JM, Tanentzap AJ. Microbiome functioning depends on individual and interactive effects of the environment and community structure. ISME J. 2018;13(1):1–11.
55. Tomasz A. Microbiology: Weapons of microbial drug resistance abound in soil flora. Science. 2006;311(5759):342–343.

56. Gottesman MM. Biochemistry of multidrug resistance mediated by the multidrug transporter. Annu Rev Biochem. 1993;62(1):385–427.
57. Zaguilán RM, Raghunand N, Lynch RM, Bellamy W, Martinez GM, Rojas B, et al. pH and drug resistance. I. functional expression of plasmalemmal V-type H^+-ATPase in drug-resistant human breast carcinoma cell lines. Biochem Pharmacol. 1999;57(9):1037–1046.
58. Chen Y, Jiang YM, Huang HY, Mou LC, Ru JL, Zhao JH, et al. Long-term and high-concentration heavy-metal contamination strongly influences the microbiome and functional genes in Yellow River sediments. Sci Total Environ. 2018;637–638:1400–1412.
59. Yuan SY, Liu C, Liao CS, Chang BV. Occurrence and microbial degradation of phthalate esters in Taiwan river sediments. Chemosphere. 2002;49(10):1295–1299.
60. Bremner JM, Tabatabai MA. Use of an ammonia electrode for determination of ammonium in Kjeldahl analysis of soils. Commun Soil Sci Plan. 1972;3:159–165.
61. Nelson DW, Sommers LE. Total carbon, organic carbon and organic matter. In: Page AL, Miller RH, Keenay DR, editors. Methods of soil analysis, part 2. Madison: American Society of Agronomy; 1982. p. 539–580.
62. Anderson JM, Ingram JSI. Tropical soil biology and fertility. In: Anderson JM, Ingram JSI. editors. A Handbook of Methods. Wallingford, UK: Centre Agriculture Bioscience International; 1989. p. 179–188.
63. Bao SD. Soil agricultural chemical elements analysis, third edition. In: Bao SD, editor. Determination methods for soil potassium. Beijing: China agriculture press; 2000. p. 106–107.
64. Noguchi H, Park J, Takagi T. MetaGene: prokaryotic gene finding from environmental genome shotgun sequences. Nucleic Acids Res. 2006;34(19):5623–
65. Fahlgren N, Howell MD, Kasschau KD, Chapman EJ, Sullivan CM, Cumbie JS, et al. High-throughput sequencing of Arabidopsis microRNAs: evidence for frequent birth and death of MIRNA genes. PLoS One. 2007;2(2):e219.
66. Altschul SF, Madden TL, Schäffer AA, Zhang J, Zhang Z, Miller W, et al. Gapped BLAST and PSI-BLAST: a new generation of protein database search programs. Nucleic Acids Res. 1997; 25(17):3389–3402.
67. Ondov BD, Bergman NH, Phillippy AM. Interactive metagenomics visualization in a web browser. BMC Bioinformatics. 2011;12:385.
68. Oksanen J, Blanchet FG, Friendly M, Kindt R, Legendre P, McGlinn D, et al. Vegan: community ecology package. R package version 2.5–6. 2019. https://cran.r-project.org/web/packages/vegan.
69. Kanehisa M, Goto S. KEGG: kyoto encyclopedia of genes and genomes. Nucleic Acids Res. 2000;28(1):27–30.
70. Qin JJ, Li RQ, Raes J, Arumugam M, Burgdorf K S, Manichanh C, et al. A human gut microbial gene catalogue established by metagenomic sequencing. Nature. 2010;464:59–65.

71. Michelsen CF, Pedas P, Glaring MA, Schjoerring JK, Stougaard P. Bacterial diversity in Greenlandic soils as affected by potato cropping and inorganic versus organic fertilization. Polar Biol. 2014;37(1):61–71.
72. Yin YN, Wang JL. Changes in microbial community during biohydrogen production using gamma irradiated sludge as inoculum. Bioresource Technol. 2016;200:217–222.
73. Caporaso JG, Kuczynski J, Stombaugh J, Bittinger K, Bushman FD, Costello EK, et al. QIIME allows analysis of high-throughput community sequencing data. Nat Methods. 2010;7:335–336.
74. Segata N, Izard J, Waldron L, Gevers D, Miropolsky L, Garrett W S, et al. Metagenomic biomarker discovery and explanation. Genome biol. 2011;12:R60.
75. Friedman J, Alm EJ. Inferring correlation networks from genomic survey data. PLoS Comput Biol. 2012;8:e1002687.
76. Zhu J, Liao M, Yao ZT, Liang WY, Li QB, Liu JL, et al. Breast cancer in postmenopausal women is associated with an altered gut metagenome. Microbiome. 2018;6:136.
77. Ofek-Lalzar M, Sela N, Goldman-Voronov M, Green SJ, Hadar Y, Minz D. Niche and host-associated functional signatures of the root surface microbiome. Nat Commun. 2014;5:4950.

Table 1

Due to technical limitations, Table 1 is provided in the Supplementary Files section.

Caption: Comparative analysis of the general characteristics in superficial soils between different intensive cropping history. Bold font values are means of three replicate with standard error (s.e.). TN: total nitrogen; OM: organic matter; AP: available phosphorus; AK: available potassium; NH4+-N: Ammonium nitrogen; NO3--N: nitrate nitrogen. Different letters denote significant differences ($p < 0.05$) among sample groups based on one-way ANOVA. V0 indicates conventional paddy fields (rice-wheat rotation, control), V10 and V20 indicate rice-vegetable rotations that were separately converted from conventional paddy 10 years and 20 years ago.

Figures

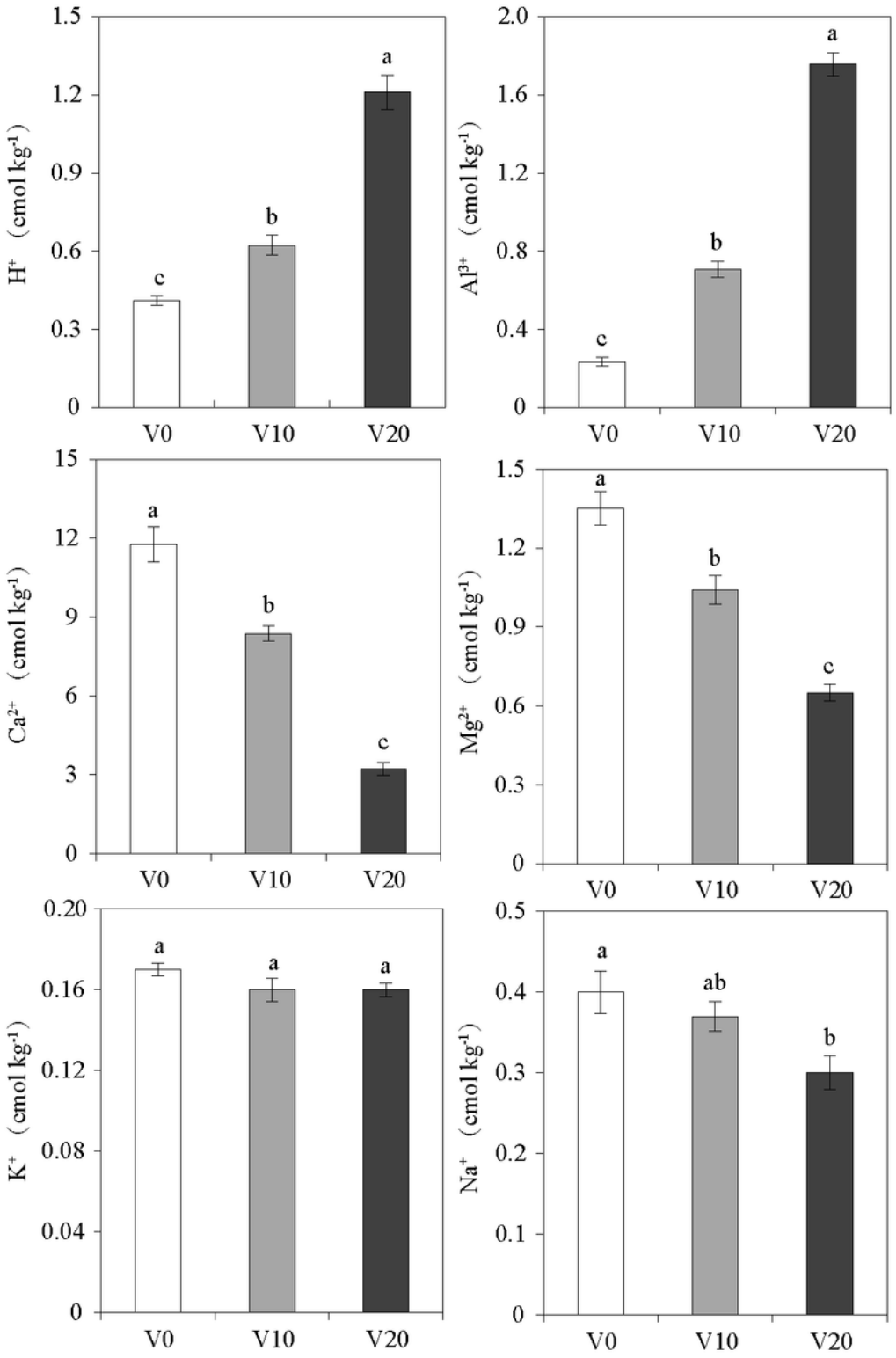

Figure 1

Soil exchangeable cation pool compositional shift over intensive cropping history. Values are means of three replicates with standard error. Different letters denote significant differences ($p < 0.05$) among sample groups based on one-way ANOVA. V0 indicates conventional paddy fields (rice-wheat rotation, control), V10 and V20 indicate rice-vegetable rotations that were separately converted from conventional paddy 10 years and 20 years ago.

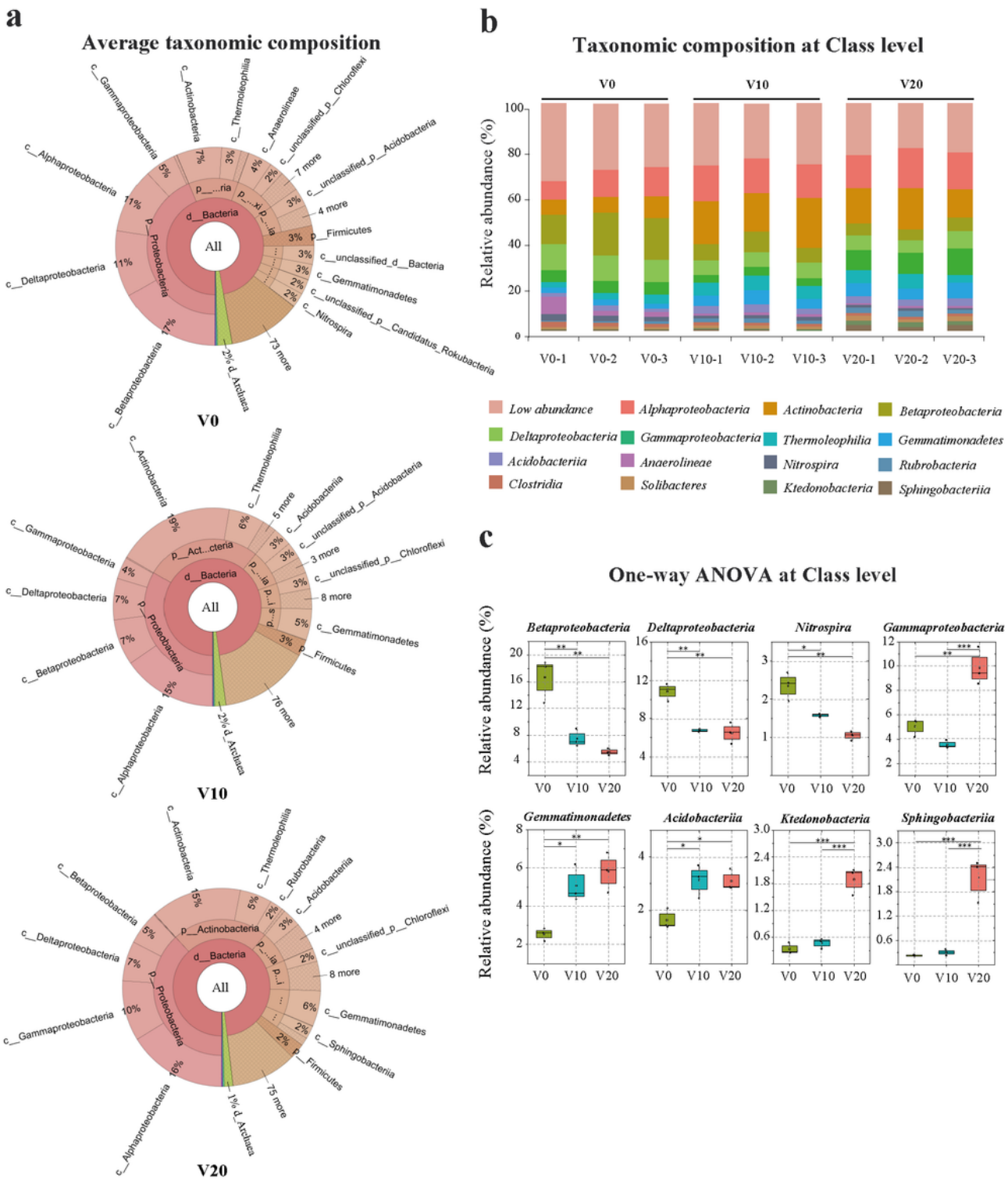

Figure 2

Metagenomic species profiling for high-order taxonomic composition. (a) Average taxonomic composition of soil microbial communities upon short- versus long-term agricultural intensification, estimated from the whole metagenome reads with BLASTP and visualized with KronaTools. (b) Class-level distribution of the microbiota across all samples. (c) The comparison of the classes with significant differences between the sample groups. Boxes represent means ± standard error; the upper and lower

whiskers represent the maximum and minimum values, respectively; the horizontal bars within boxes represent medians; squares represent means; significance bars represent group significance based on one-way ANOVA, and stars denote the p-value thresholds (* = 0.05, ** = 0.01, *** = 0.001).

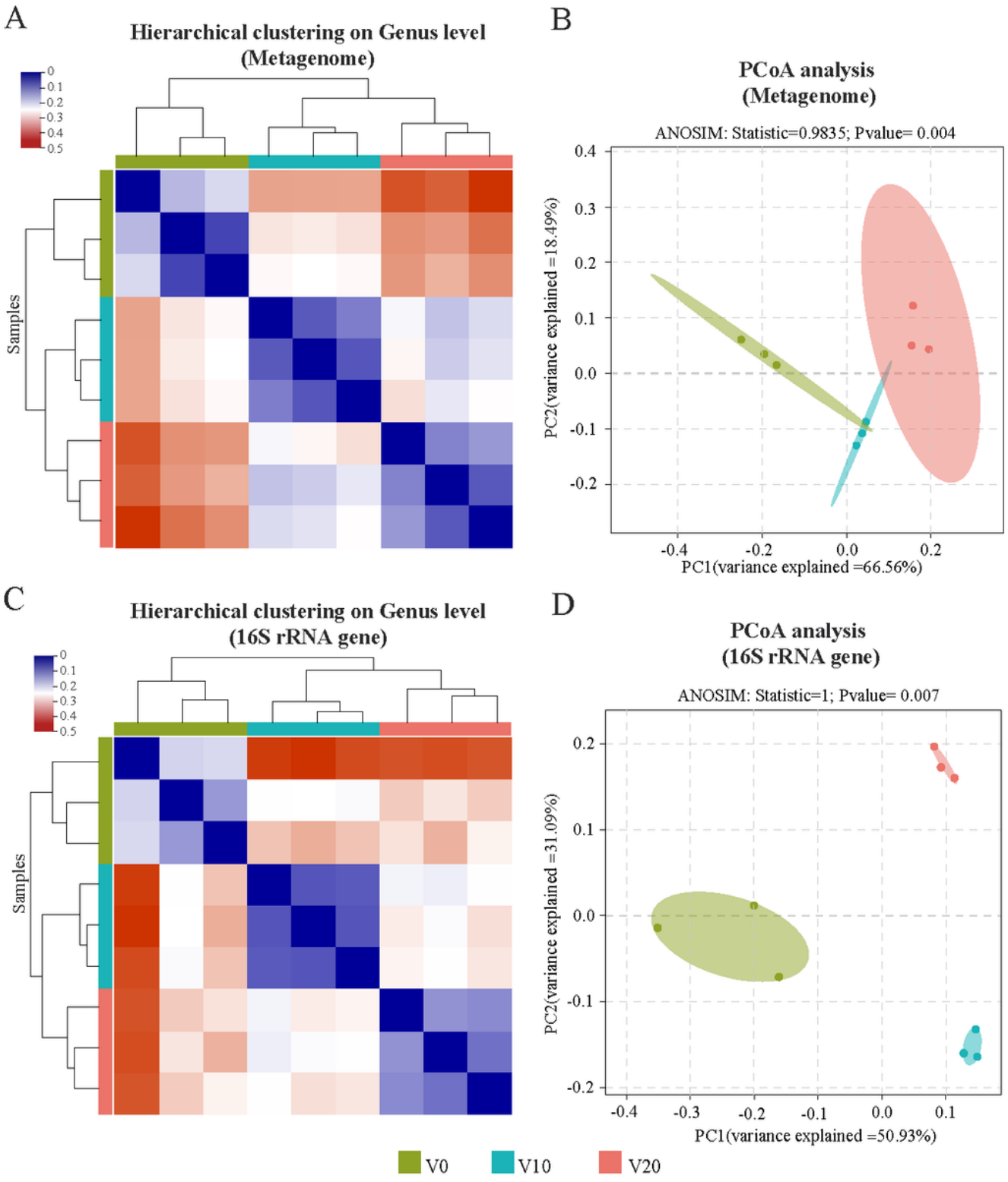

Figure 3

Dissimilarity clustering of soil microbiomes between different intensive cropping history (fine-scale). (a) Genus-level hierarchical clustering (Bray-Curtis distances) and (b) principal co-ordinates analysis (PCoA)

of sample groups, based on standardized relative abundance of metagenomic species. (c) Genus-level hierarchical clustering (Bray-Curtis distances) and (d) PCoA of sample groups, based on 16S rRNA gene amplicon sequencing of Bacteria. Differences in intergroup and between-group based on analysis of similarities (ANOSIM) with Bray-Curtis distance (b, d).

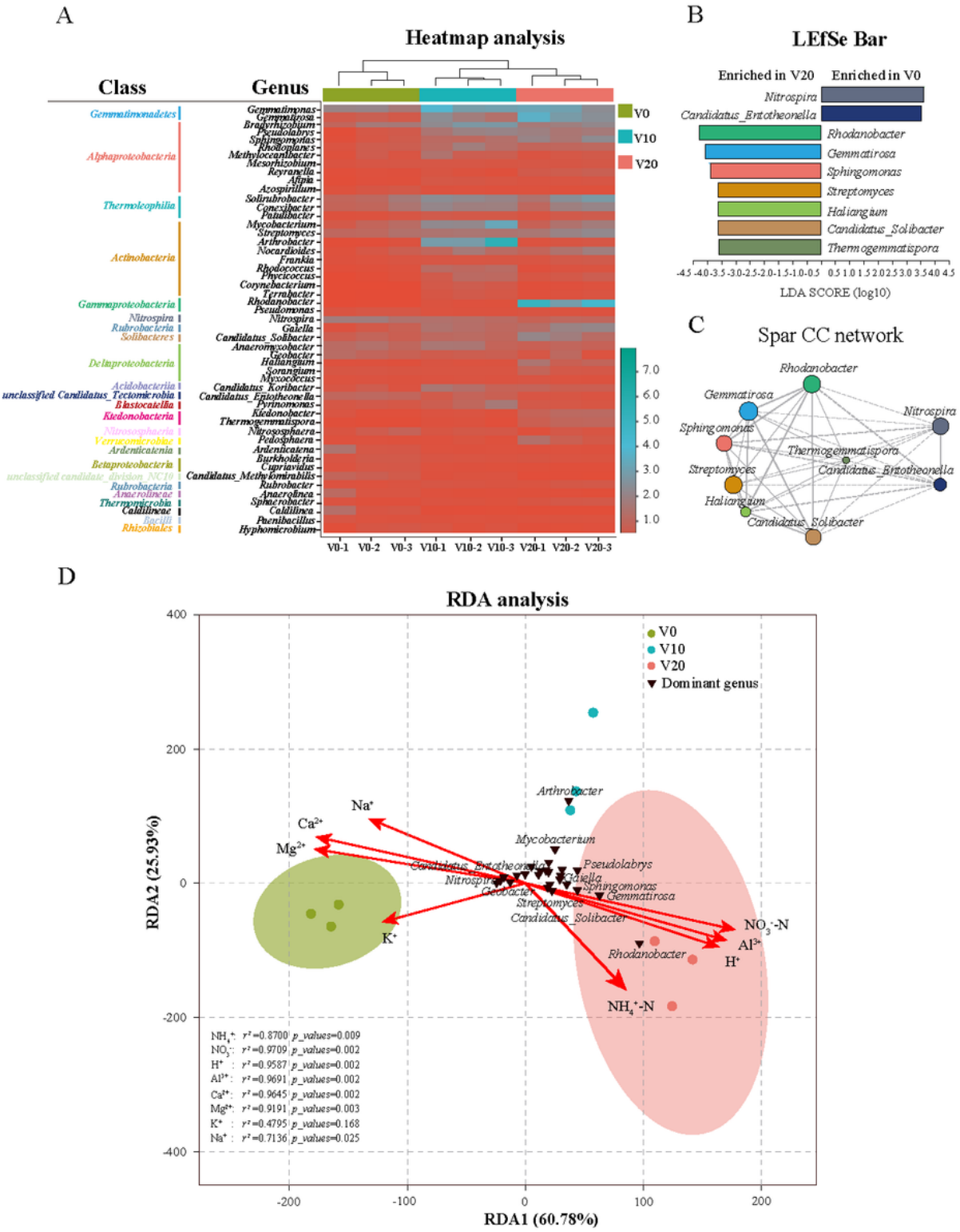

Figure 4

Classification to identify the biomarkers of soil microbiome in different intensive cropping history. (a) Taxonomic comparison of the 50 most abundant genera and its classes across all samples. (b) Histogram of the linear discrimination (LDA) scores computed for genera differentially abundant between V0 and V20. (c) SparCC network plot of co-abundance and co-exclusion correlations between differentially abundant biomarkers. Each node represents a genus and its dimension is proportional to the mean relative abundance within the population. Two nodes are linked if the correlation was significant (p-value thresholds=0.05), and thickness gradient of lines indicates the magnitude of Spearman's rank correlation coefficient. (d) Redundancy analysis (RDA) of microbial community, acidity parameters and samples. The inverted triangle indicates the dominant genera, and twelve of which with high correlation were listed by italics.

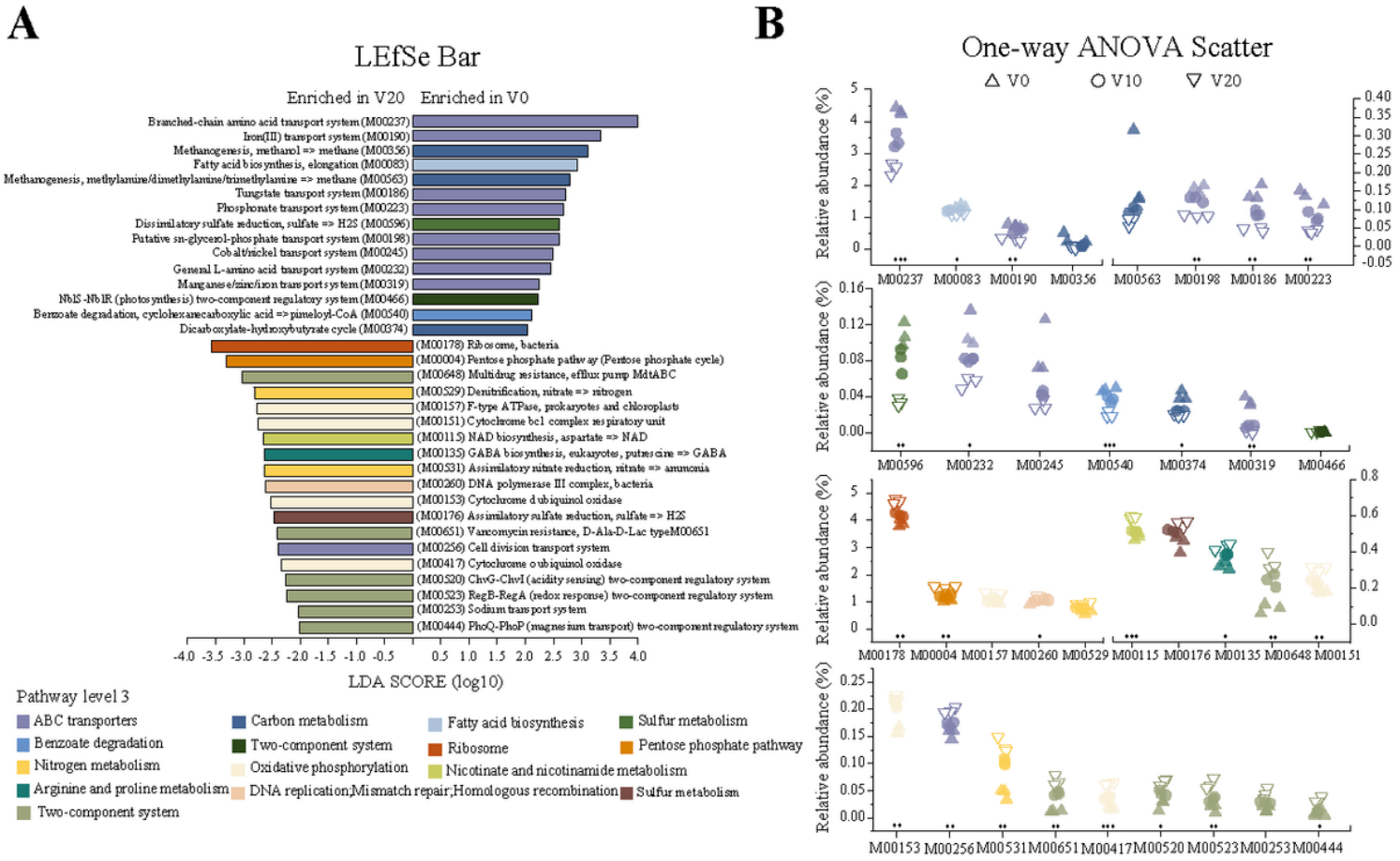

Figure 5

Classification to identify the indicative functions of soil microbiome in different intensive cropping history. (a) Histogram showing the most representative part of indicative modules enriched in V0 or V20, indicative modules that LDA scores (log 10) of 2 or greater are listed in additional file 2: Fig. S2. (b) One-way ANOVA reveals differentially abundance of indicative modules between groups, and stars denote the p-value thresholds (* = 0.05, ** = 0.01, *** = 0.001).

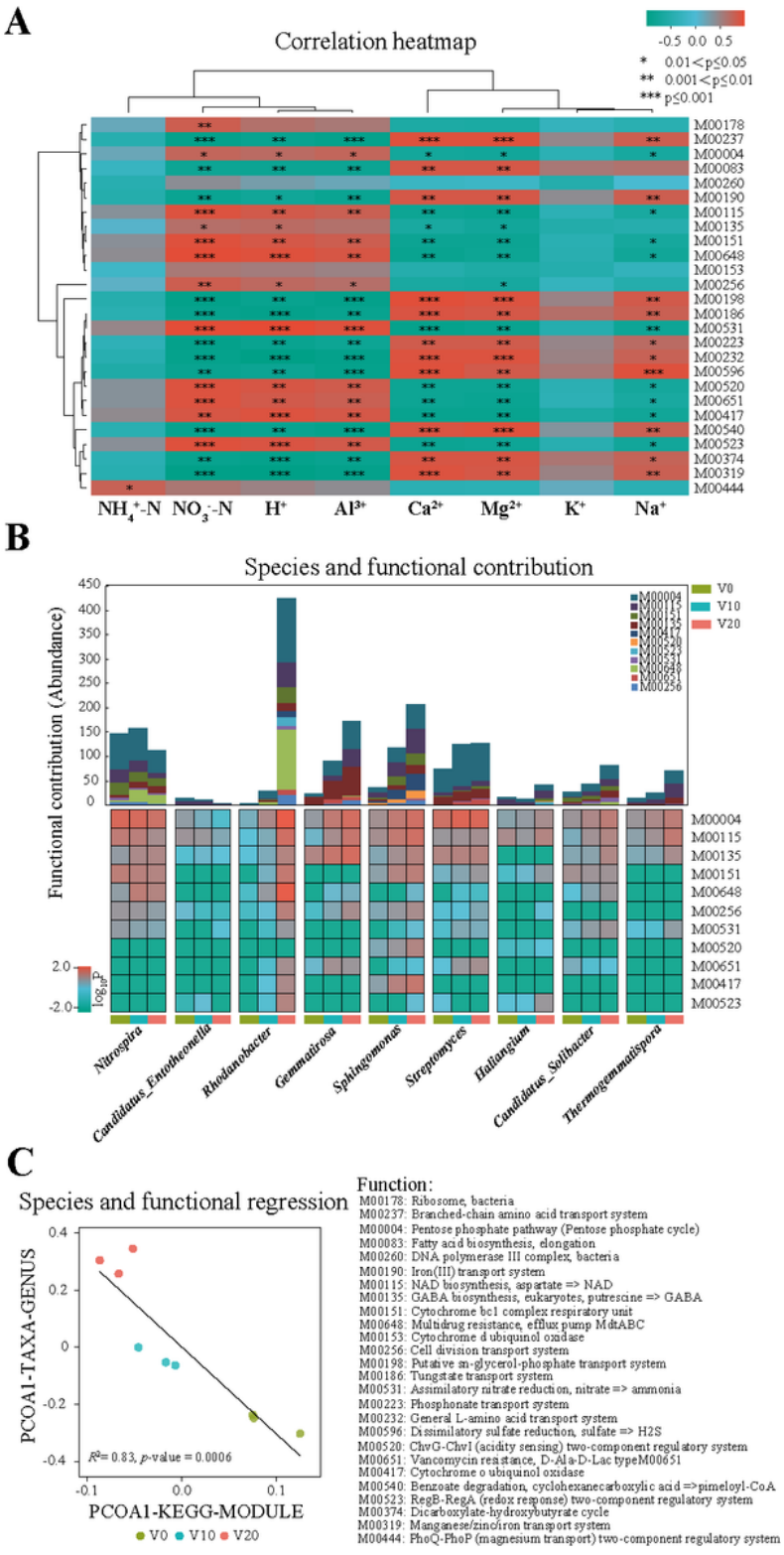

Figure 6

Correlation between indicative functions and chemical indices of soil acidification, its contributions to the biomarkers. (a) Identification of the correlation between indicative modules and acidity parameters. Spearman's rank correlation coefficient is indicated by a color gradient: red indicates positive correlation; green, negative correlation; stars denote the p-value thresholds. (b) Contribution of identified pH

homeostasis modules to acid-sensing biomarkers. (c) The similarity in pH homeostasis modules and acid-sensing biomarkers community composition.

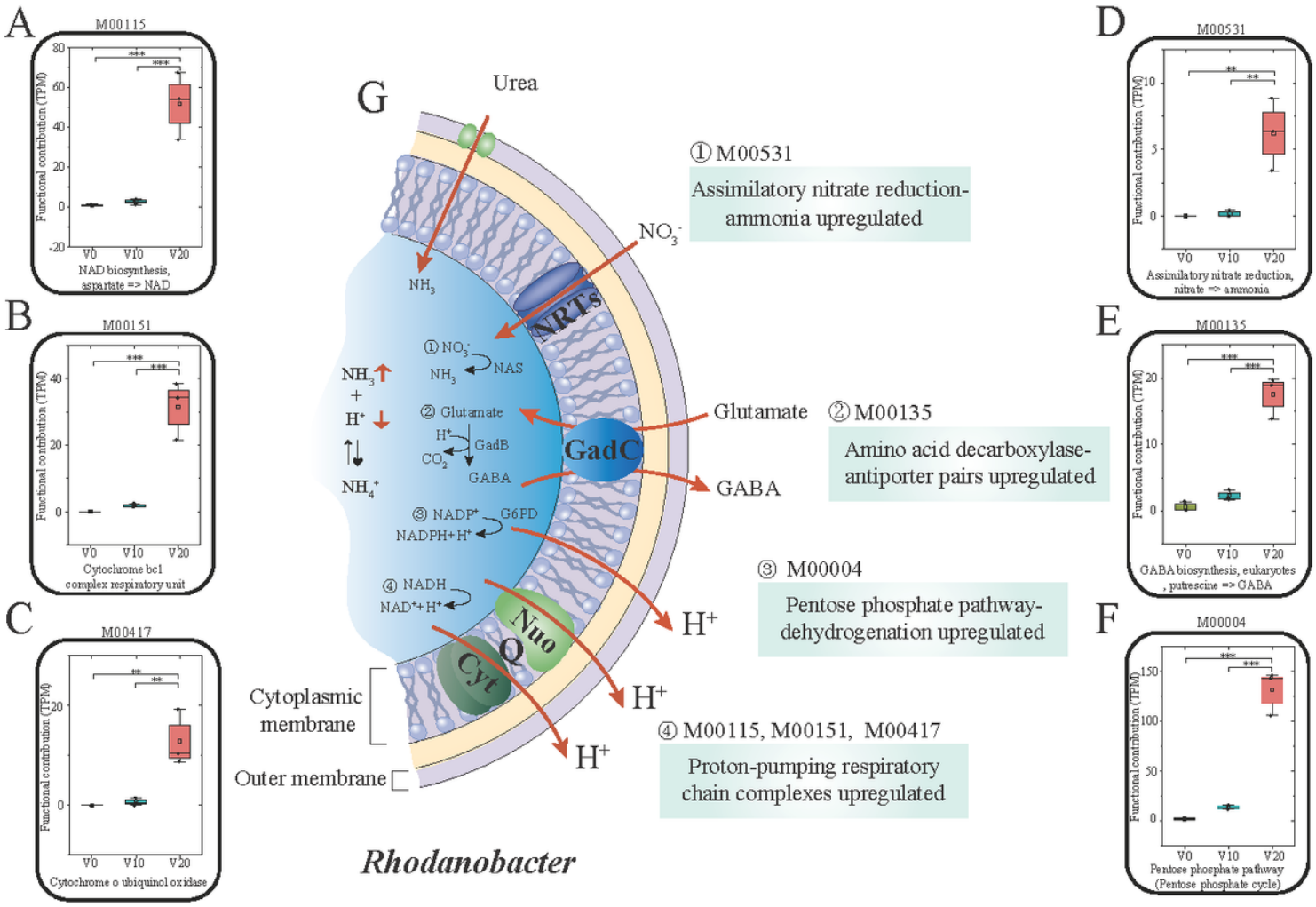

Figure 7

Schematic map shows potential pH homeostasis pathways of Rhodanobacter. (a) ~ (f) One-way ANOVA box plots show the differences in contribution of pH homeostasis modules among sample groups. Boxes represent means±standard error; upper and lower whiskers represent the maximum and minimum values, respectively; horizontal bars within boxes represent medians; squares represent means; significance bars represent group significance based on one-way ANOVA, and stars denote the p-value thresholds (* = 0.05, ** = 0.01, *** = 0.001). (g) Major pH homeostasis strategies that supporting acid tolerance of Rhodanobacter. NRTs, nitrate transporter; NAS, assimilatory nitrate reductase; GadC, glutamate/γ-aminobutyrate antiporter; GadB, γ-aminobutyric acid; GABA, γ-aminobutyric acid; G6PD, glucose 6-phosphatedehydrogenase; NADP/NADPH, nicotinamide adenine dinucleotide phosphate; Nuo, NADH–ubiquinone oxidoreductase; Cyt, cytochrome complex; Q, quinone pool; NAD/NADH, nicotinamide adenine dinucleotide.

Supplementary Files

This is a list of supplementary files associated with this preprint. Click to download.

- Additionalfile1.xlsx
- Additionalfile3.xlsx
- Table.1.xlsx
- Additionalfile2.xlsx